dc dynamic and static pull-in predictions and analysis for electrostatically actuated clamped circular micro-plates based on a continuous model

2010 J. Micromech. Microeng. 20 025013

(http://iopscience.iop.org/0960-1317/20/2/025013)

J. Micromech. Microeng. **20** (2010) 025013 (15pp) doi:10.1088/0960-1317/20/2/025013

dc dynamic and static pull-in predictions and analysis for electrostatically actuated clamped circular micro-plates based on a continuous model

Lun-De Liao[1], Paul C-P Chao[1,2,3], Chih-Wei Huang[1] and Chi-Wei Chiu[1]

[1] Department of Electrical Engineering, National Chiao Tung University, Hsinchu 300, Taiwan
[2] Institute of Imaging and Biomedical Photonics, National Chiao Tung University, Hsinchu 300, Taiwan

E-mail: pchao@mail.nctu.edu.tw

Received 21 October 2009
Published 18 December 2009
Online at stacks.iop.org/JMM/20/025013

Abstract

This study develops a continuous model to analyze the 'pull-in' effect in the circular micro-plates used in capacitive-type micro-electro-mechanical systems (MEMS) sensors, actuators and microphones. In developing the model, the governing equation of motion of the deformed plate is established in the form of a partial different equation (PDE) which is then decomposed using the Galerkin method to create a coupled set of modal ordinary differential equations. By considering the first-order deflection mode only and using a fifth-order Taylor series expansion of the electrostatic force, closed-form solutions are obtained for both the position and the voltage of the static pull-in event. Applying an energy balance method and a finite-order approximation method, the solutions are then obtained for the position and voltage of the dynamic pull-in event. The theoretical results obtained for the pull-in phenomena are verified based on the comparison to available experimental data, and also numerically using a finite element analysis (FEA) approach. In general, the results indicate that the ratio of the dynamic to static pull-in voltages is approximately 92%. However, when the squeezed-film effect induced by the air gap between the two plates is taken into account, the value of this ratio increases slightly as a result of considering a higher dynamic pull-in voltage.

(Some figures in this article are in colour only in the electronic version)

1. Introduction

Recent advances in the MEMS field have facilitated the design and application of a variety of micro-sensors and actuators based on electrostatic actuation mechanisms. MEMS-based electrostatic devices are essentially simple capacitors composed of two parallel micro-plates, typically with a square, circular or beam-type configuration. The device is designed such that one of these plates is free to move, while the back plate remains fixed. When a voltage is applied across the two plates, an electrostatic force is induced between them, causing the deformable electrode to deflect toward the back plate. Given a sufficient intensity of the applied voltage, the electrostatic force exceeds the elastic restoring force developed within the deformed plate, and thus it collapses and makes contact with the back plate. In certain MEMS-based capacitive-type applications, e.g. microphones [1, 2] and pressure sensors [3, 4], it is essential to avoid this 'pull-in' effect since the contact between the two plates induces a short circuit and therefore renders the device inoperable. However, in other applications, e.g. optical/RF switches [5, 6], the bias voltage is deliberately tuned in such a way that the deformable plate collapses, thereby turning the switch on (or off). Therefore, the realization of such devices requires not only the availability of mature fabrication techniques, but also an in-depth knowledge of the dynamic behavior of the device structure such that the pull-in effect between the two plates can be either avoided or induced depending upon the

[3] Author to whom any correspondence should be addressed.

particular application. To these ends the critical bias voltage at which pull-in voltage and the corresponding deflection of the plates/beams (i.e. the so-called pull-in position) must be precisely computed in advance such that designers can ensure that the device will operate in accordance with the specification requirements.

The literature contains many investigations into the pull-in effect in a variety of electrostatic sensors and actuators. In some cases, a simple 1-D lumped dynamic model was used to approximate the behavior of the deformed plate in order to predict the bias voltage at which the static pull-in event occurs and the corresponding deflection of the plate (i.e. the pull-in voltage and the pull-in position, respectively) [7, 8]. However, the use of a lumped model inevitably limits the accuracy of the prediction results, and thus other researchers proposed the use of more sophisticated continuous models [9, 10] or finite element models (FEM) [8, 10, 11] to analyze the response of the deformed plate. Among the works using continuous models, they are aimed to obtain analytical predictions on the static pull-in position and voltages. For example, Younis *et al* [9] presented a continuous reduced-order model for predicting the static pull-in voltage and position of electrically actuated MEMS micro-beams. Chao *et al* [10] developed a novel computational procedure for predicting the static pull-in event and verified the numerical results experimentally. Adopting a similar approach to that employed in [11], Vogl and Nayfeh [12] presented a continuous reduced-order model with a uniform residual biaxial plane stress consideration for actuated.

All the studies described above considered the case of a static pull-in event, i.e. the intensity of the applied voltage was gradually increased until the deflection of the plate reached the critical pull-in position and caused the plate to collapse. However, in practical electrically actuated MEMS devices, the voltage applied across the two plates does not gradually increase in this manner, but changes instantaneously from zero to the specified design value. Under these conditions, the deformed beam or plate tends to overshoot the equilibrium position as a result of inertial effects, and thus it collapses at a lower voltage than that observed in the static case. Clearly, this phenomenon has considerable practical implications regarding the performance of the device, and hence many researchers have investigated the corresponding 'dynamic pull-in' phenomena. For example, Neilson and Barbastathis [13] used a lumped model to derive the dynamic pull-in voltages of parallel-plate and torsional electrostatic MEMS-based actuators, respectively. Similarly, Elata and Bamberger [14] established the dynamic pull-in voltage of a multiple degree-of-freedom parallel-plate system with multiple voltage sources. In both cases, it was shown that the ratio of the dynamic pull-in voltage to the static pull-in voltage was of the order of 91.9%.

In general, the MEMS devices in a circular plate yield better structure flexibility than rectangular plates since no corner and/or sharp edges induce higher residual stress after multiple depositions [8, 12]. As a result, they are an ideal solution for capacitive-type MEMS-based microphones and pressure sensors to render higher sensitivity. However, a review of the literature reveals that the dc dynamic pull-in characteristics of edge-clamped parallel circular plates have yet to be rigorously explored. Accordingly, the objective of the current study is to develop a continuous model of the edge-clamped parallel circular plate structure such that accurate predictions of both its static and its dynamic pull-in characteristics can be obtained. The study commences by establishing the equation of motion of the edge-clamped deformable micro-plate in the form of a partial differential equation (PDE). Using the Galerkin method, the PDE is then decomposed into a coupled set of modal ordinary differential equations (ODEs). Taking a first-mode approximation and using a fifth-order Taylor's expansion method to facilitate the computation of the distributed electrostatic force, closed-form solutions are derived for the voltage and position of the static pull-in event. Subsequently, an energy balance method [13, 20] is employed to derive closed-form expressions for the voltage and position of the dynamic pull-in event for the ideal case where the parallel circular plate system has no damping effects. Finally, a finite-order approximation method is proposed for deriving the dynamic pull-in phenomena of a realistic parallel circular plate system in which the deformation of the plate is opposed by a squeezed-film effect generated by the air in the gap between the two plates. The various theoretical models are used to evaluate the respective effects of the plate radius, the plate thickness and the air gap height on the static and dynamic pull-in voltages and positions of the parallel plate system. The influence of the squeezed-film damping effect on the pull-in phenomena is also systematically explored. Finally, the theoretical results are compared with available experimental data in [12], and validated numerically using a finite element analysis (FEA) approach.

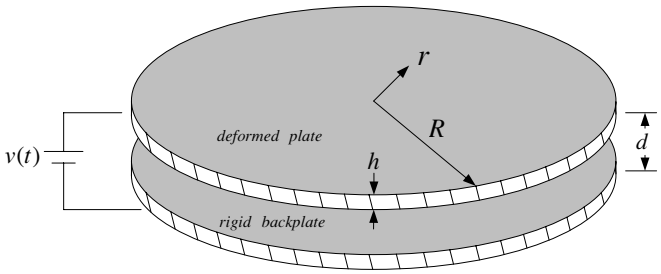

Figure 1. Schematic illustration showing the electrostatic actuation of the parallel edge-clamped circular micro-plates.

2. Modeling

2.1. Model description

Figure 1 illustrates the configuration of the two edge-clamped parallel circular micro-plates considered in the present analysis. When a voltage, $v(t)$, is applied between the upper and lower plates at time t, the resulting electrostatic force induced between them causes the upper plate to deflect toward the lower plate. At a certain value of the bias voltage, the magnitude of the attractive force between the

two plates exceeds that of the restoring force developed within the deflected plate, and thus a pull-in event takes place. As described in the introduction, it is essential that this pull-in event can be accurately predicted during the design stage such that appropriate parameter values can be assigned to the parallel plate structure in order to either prevent or induce the pull-in effect, depending upon the particular application.

While predicting the pull-in voltage, it is necessary to establish the governing equation of motion of the upper, deformable plate. Since this plate is radially symmetrical, the governing equation of motion can be expressed as follows [15]:

$$\rho h\frac{\partial^2 w}{\partial t^2}+2c\frac{\partial w}{\partial t}+D\nabla^4 w=\frac{1}{r}\frac{\partial}{\partial r}\left(\frac{\partial w}{\partial r}\frac{\partial \Phi}{\partial r}\right)+\frac{\tau h}{r}\frac{\partial}{\partial r}\left(r\frac{\partial w}{\partial r}\right)+F_e, \tag{1}$$

where

$$\nabla^4 w=\left(\frac{\partial^2}{\partial r^2}+\frac{1}{\hat{r}}\frac{\partial}{\partial r}\right)\left(\frac{\partial^2 w}{\partial r^2}+\frac{1}{\hat{r}}\frac{\partial w}{\partial r}\right), \tag{2}$$

In equations (1) and (2), ρ is the density of the plate material; h is the plate thickness; c is the damping coefficient of the plate material; D is the flexural rigidity of the plate; ∇^4 is the biharmonic operator, $w = w(r, t)$ is the deflection of the deformed plate, where r is the radial coordinate of the plate and t denotes time; $\Phi(r, t)$ is the stress function; and τ is the uniform residual biaxial plane stress per unit distance of the deformed plate. From basic principles, the flexural rigidity of the plate, D, can be formulated as

$$D=\frac{Eh^3}{12(1-\nu^2)}, \tag{3}$$

where E and ν are Young's modulus and Poisson ratio of the deformed plate, respectively. The term F_e in equation (1) denotes the electrostatic force acting on each unit area of the circular plate when a bias voltage is applied and can be expressed as

$$F_e=\frac{\varepsilon V_b^2}{2(d-w)^2}, \tag{4}$$

where V_b is the bias voltage; d is the height of the air gap between the two plates; and ε is the permittivity of air. Note that the electrostatic force given in equation (4) provides an approximation of the capacitance between two edge-clamped parallel plates for which the fringing fields at the boundary are ignored [16].

The boundary conditions for the governing equation of the upper edge-clamped circular plate in the absence of an electrostatic force are given by

$$w(R,t)=0, \tag{5}$$

$$\frac{\partial w(R,t)}{\partial r}=0, \tag{6}$$

$$\Phi(r,t)=0. \tag{7}$$

Note that equations (5) and (6) indicate that the edge of the plate is clamped, while equation (7) indicates that the plate is in a non-stressed condition. For analytical convenience, equation (1) can be non-dimensionalized using the following parameters:

$$\hat{w}=\frac{w}{d},\qquad \hat{r}=\frac{r}{R},\qquad \hat{t}=t\sqrt{\frac{D}{\rho h R^4}},$$
$$\hat{c}=c\frac{R^2}{\sqrt{\rho h D}},\qquad \hat{\tau}=\tau\frac{hR^2}{D},\qquad \alpha=\frac{\varepsilon R^4}{Dd^3}, \tag{8}$$
$$\hat{V}_b=\frac{V_b}{V_0}\quad\text{and}\quad \hat{F}_e=\frac{V_b}{2(1-\hat{w})^2}.$$

The governing equation of motion of the upper plate can then be rewritten in the form

$$\frac{\partial^2 \hat{w}}{\partial \hat{t}^2}+2\hat{c}\frac{\partial \hat{w}}{\partial \hat{t}}+\hat{\nabla}^4\hat{w}=\hat{\tau}\frac{1}{\hat{r}}\frac{\partial}{\partial \hat{r}}\left(\hat{r}\frac{\partial \hat{w}}{\partial \hat{r}}\right)+\alpha\hat{F}_e, \tag{9}$$

where

$$\hat{\nabla}^4\hat{w}=\left(\frac{\partial^2}{\partial \hat{r}^2}+\frac{1}{\hat{r}}\frac{\partial}{\partial \hat{r}}\right)\left(\frac{\partial^2 \hat{w}}{\partial \hat{r}^2}+\frac{1}{\hat{r}}\frac{\partial \hat{w}}{\partial \hat{r}}\right).$$

The corresponding non-dimensional boundary conditions are given by

$$\hat{w}(1,\hat{t})=0, \tag{10}$$

$$\frac{\partial \hat{w}(1,\hat{t})}{\partial \hat{r}}=0, \tag{11}$$

$$\Phi(\hat{r},\hat{t})=0. \tag{12}$$

Having derived the governing equation and its boundary conditions, the static and dynamic pull-in characteristics of the two-plate system can be facilitated by performing a modal decomposition of equation (9), as demonstrated in the following section.

2.2. Reduced-order model

In the current study, the governing PDE given in equation (9) is decoupled using the Galerkin method [17] to create a coupled set of discrete modal ODEs. The decoupling process commences by separating the deformation of the upper circular plate into its temporal components, $w_k(\hat{t})$, and its spatial components, $\phi_k(\hat{r})$, respectively. The deflection, $\hat{w}(\hat{r},\hat{t})$, can then be expressed in the form of a series of products of these two components, i.e.

$$\hat{w}(\hat{r},\hat{t})\approx\sum_{k=1}^{N} w_k(\hat{t})\phi_k(\hat{r}),\qquad 1\leqslant k\leqslant N \tag{13}$$

where $w_k(\hat{t})$ is the kth time-dependent generalized coordinate of the kth mode shape function, $\phi_k(\hat{r})$ is the kth radial-dependent mode shape function and satisfies the boundary conditions given in equations (11) and (12) and N is the number of modes considered. As N approaches infinity, the approximation given in equation (13) becomes exact provided that the specified mode shape function forms a complete set.

If the mode shape function,$\phi_k(\hat{r})$, is specified as the axi-symmetric modes of the deformed plate, it can be shown that the mode shapes are given by [15]

$$\phi_k(\hat{r})=C_k\left(\frac{J_0(\hat{r}\sqrt{\Omega_k})}{J_0(\sqrt{\Omega_k})}-\frac{I_0(\hat{r}\sqrt{\Omega_k})}{I_0(\sqrt{\Omega_k})}\right), \tag{14}$$

where J_0 is the Bessel function of the first kind, I_0 is the modified Bessel function of the first kind [18], C_k is a constant coefficient corresponding to the$k$th mode shape and Ω_k is the kth natural frequency. Applying the same procedure of the well-known Galerkin method, substituting equation (13) into equation (9), multiplying both sides by the mode shape function in equation (14) and integrating the substituted equations over the surface domain of the deformed thin circular plate, the coupled set of nonlinear modal ODEs describing the parallel micro-plate structure can be derived as

$$\mathbf{M}\ddot{\mathbf{w}} + \mathbf{C}\dot{\mathbf{w}} + \mathbf{K}\mathbf{w} = \mathbf{f_e}, \tag{15}$$

where $\mathbf{w}$ contains all $w_k(\hat{t})$, $1 \leqslant k \leqslant N$. The individual terms within equation (15) are given by

$$m_k = \int_0^1 \phi_k^2 \, \mathrm{d}\hat{r}, \tag{16}$$

$$c_k = 2\hat{c} \int_0^1 \phi_k^2 \, \mathrm{d}\hat{r}, \tag{17}$$

$$k_k = \left[\left(\frac{\partial^2}{\partial \hat{r}^2} + \frac{1}{\hat{r}} \frac{\partial}{\partial \hat{r}} \right) \left(\frac{\partial^2 \phi_k}{\partial \hat{r}^2} + \frac{1}{\hat{r}} \frac{\partial \phi_k}{\partial \hat{r}} \right) - \hat{\tau} \frac{1}{\hat{r}} \frac{\partial}{\partial \hat{r}} \left(\hat{r} \frac{\partial \phi_k}{\partial \hat{r}} \right) \right]. \tag{18}$$

In the system equation given in equation (15), the electrostatic force term, $\mathbf{f_e}$, has the form

$$f_{e,k} = \alpha \int_0^1 \hat{F}_e \phi_k \, \mathrm{d}\hat{r}, \tag{19}$$

where $\hat{F}_e$ is the distributed electrostatic force between the two parallel circular plates and varies as a nonlinear function of the upper plate deflection. Observing equations (15)–(19), a number of significant points emerge. First, kth derived are in fact the natural frequencies associated with the eigenmodes of the deformed circular plate. Second, the orthogonality existing between different modes results in diagonal matrices **M**, **C** and **K**, as evidenced from the computed right-hand sides of equations (16), (17) and (18), respectively. In other words, the left-hand side of equation (15) is decoupled. Furthermore, since the computed entries of matrices **M**, **C** and **K**are constant, all of the terms on the left-hand side of the reduced equation (15) are linear. Third, the modal electrostatic force vector, $\mathbf{f_e}$, is computed by integrating the nonlinear distributed electrostatic force $\hat{F}_e$ given in equation (4). The nonlinear dependence of $\hat{F}_e$ on the circular plate deflection $\hat{w}(\hat{r}, \hat{t})$ renders $\mathbf{f_e}$ the only coupled and nonlinear term in equation (15).

It should be noted at this point that having computed matrices **M**, **C** and **K**, the only term remaining to be evaluated is the electrostatic force acting on the deformable plate, i.e. $\mathbf{f_e}$. However, performing the integration operation in equation (19) is complex due to the nonlinearity of the electrostatic force term, $\hat{F}_e$. In practice, equation (19) can be solved in one of two different ways, namely using a numerical method to perform a full-order Gaussian integration; or (2) performing a finite-order Taylor series expansion of the electrostatic force, $\hat{F}_e$, prior to carrying out the integration operation. The integration results based on the Taylor series expansion enable a closed-form prediction of the pull-in position/voltage. The results of the Gaussian integration process can be used to help determine the order of the Taylor series required to obtain an accurate closed-form approximation of the pull-in position/voltage. For example, considering only the first mode in equation (13), the corresponding electrostatic force, $f_{e,1}$, is computed using both methods. Figure 2 compares the results obtained by the two methods for the variation of the electrostatic force as a function of the steady-state deflection of the plate center. Note that in computing the results, both methods consider only the first deflection mode (w_1) in equation (13). It can be seen that the approximation results obtained using the fifth-order Taylor series expansion method are very close to the numerical results obtained using the full-order Gaussian integration method for the case where w_1 is less than 0.5. As will be shown later, the static pull-in position is invariably less than 0.5, and thus in the current analysis, equation (19) is solved using the fifth-order Taylor series expansion approach. This strategy avoids the requirement for a numerical scheme to process the full-order Gaussian integration of $\hat{F}_e$ and yields closed-form approximations of the pull-in voltage and pull-in position which are in very close agreement with the exact results.

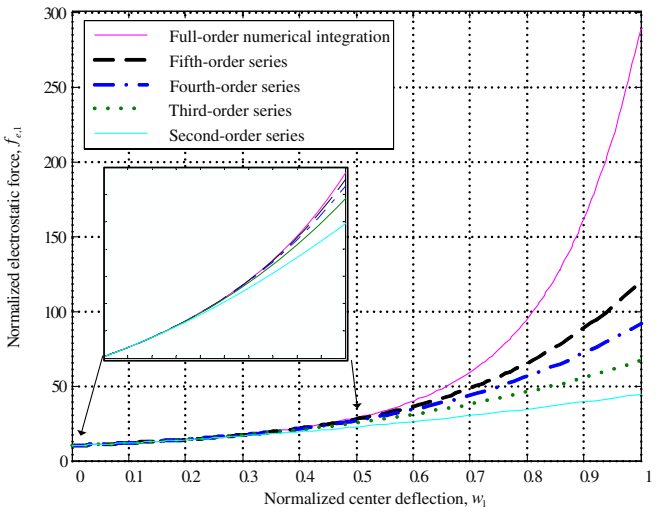

Figure 2. Full-order and finite-order solutions for variation of electrostatic force with respect to the deflection in the center of the deformed circular plate.

3. Pull-in prediction

This section employs the continuous model developed in section 2 to predict the static and dynamic pull-in voltages and positions of the deformable plate shown in figure 1 for various values of the plate thickness, the plate radius and the air gap height.

3.1. Static pull-in prediction

In analyzing the deformation of the circular micro-plate, the present analysis considers only the first mode of the decoupled

system equation given in equation (13). It will be shown later in section 5 that this first-mode approximation is entirely adequate for the purposes of predicting the deflection of the center point of the deformed circular plate. The pull-in event can be predicted by analyzing the static equilibrium between the elastic restoring force developed within the deformed circular plate, i.e. the third term on the left-hand side of equation (15), and the electrostatic force induced by the applied bias voltage, i.e. the right-hand side of equation (15), i.e.

$$f_{r,1} = f_{e,1}, \tag{20}$$

where $f_{r,1}$ is the net restoring force associated with the first deflection mode, while $f_{e,1}$ is the corresponding electrostatic force. From equation (18), the restoring force, $f_{r,1}$, can be obtained as

$$f_{r,1} = k_1 w_1, \tag{21}$$

where w_1 denotes the normalized steady-state first-mode deflection of the center point of the deformed circular plate. Meanwhile, $f_{e,1}$ can be derived by integrating equation (19) with $k = 1$. At the moment that the static pull-in event occurs, the rate of change of the electrostatic force, $f_{e,1}$, with respect to the deflection of the circular plate, w_1, is equal to that of the restoring force $f_{r,1}$, i.e.

$$\frac{\partial f_{r,1}}{\partial w_1} = \frac{\partial f_{e,1}}{\partial w_1}, \tag{22}$$

which means that the tangency of the electrostatic force $f_{e,1}$ and the restoring force $f_{r,1}$ are equal with respect to circular plate center deflection w_1. The pull-in position and pull-in voltage can therefore be found by solving equations (20) and (21) simultaneously, yielding

$$f_{e,1} \cdot \frac{\partial f_{r,1}}{\partial w_1} = f_{r,1} \frac{\partial f_{e,1}}{\partial w_1}. \tag{23}$$

where it is seen that w_1 is the only unknown to be solved in determining the pull-in position. In other words, the pull-in position is independent of the magnitude of the applied bias voltage.

As described in section 2, the electrostatic force terms in equation (23) can be solved using either a finite-order Taylor series expansion method or a full-order numerical scheme. Using a fifth-order Taylor series expansion to approximate $f_{e,1}$ and $\frac{\partial f_{e,1}}{\partial w_1}$ yields an expression of the form

$$\begin{aligned} f_{e,1}\frac{\partial f_{r,1}}{\partial w_1} - f_{r,1}\frac{\partial f_{e,1}}{\partial w_1} \cong{}& \alpha \hat{V}_b^2 C_1^2 \cdot (441.759 + 34.6101\hat{\tau}) \\ & \cdot \left[-0.256\,582 + 0.484\,726 w_1^2 - 1.132\,33 w_1^3 \right. \\ & \left. + 1.912\,15 w_1^4 - 2.8058 w_1^5\right] = 0. \end{aligned} \tag{24}$$

This equation can be solved by setting the sum of the terms in the brackets equal to zero, resulting in a normalized value of the pull-in position, i.e. a value describing the deflection of the center point of the circular plate as a ratio of the total height of the air gap. From inspection, the normalized pull-in position is found to have a value of

$$w_{1,pi} \approx 0.415. \tag{25}$$

Figure 3 illustrates the variations of the restoring force and the electrostatic force, respectively, as the normalized deflection

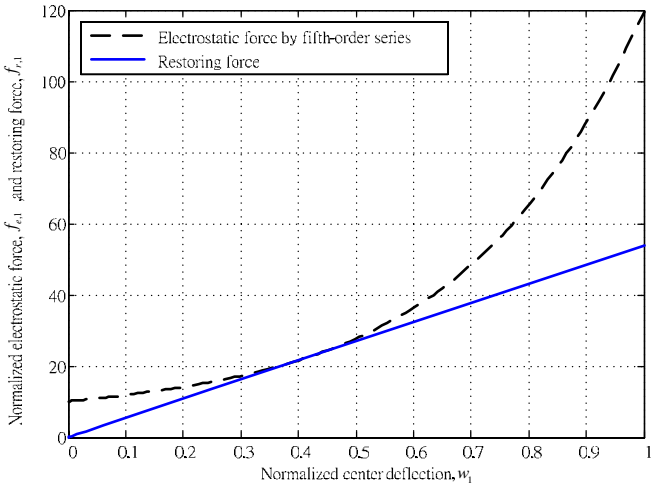

Figure 3. Variations of the fifth-order Taylor series approximation of electrostatic force and restoring force, respectively, with respect to the normalized deflection in the center of the deformed circular plate. (Note: point of tangency at $w_{1,pi} \approx 0.415$.)

of the center point of the deformed plate is progressively increased. As shown, the two profiles are tangent at a deflection value of 0.415, corresponding to the normalized pull-in position. From equation (25), it is apparent that the normalized pull-in position is not only independent of the bias voltage, but also of all the system parameters, namely the radius and thickness of the plate, the plate material, the height of the air gap and so forth. Therefore, the normalized pull-in position of $w_{1,pi} \approx 0.415$ predicted based on a continuous model corresponds to a smaller gap between two charged plates at the occurrence of pull-in.

As indicated above, the electrostatic force terms in equation (23) can also be solved by conducting a full-order numerical integration operation. Adopting this approach, the normalized value of the pull-in position is found to be 0.408. Figure 4 illustrates the results obtained for the pull-in position by the full-order numerical method and the finite-order Taylor series expansion approach, respectively. In general, both sets of results indicate that the value of the normalized pull-in position is independent of the radius of the circular plate. Thus, it is shown that the pull-in phenomenon is well predicted, and furthermore, it can be seen that the prediction of the normalized pull-in position obtained using the fifth-order Taylor expansion method is in good agreement with the results obtained using the full-order numerical integration scheme.

Having established the value of the normalized pull-in position, the corresponding pull-in voltage is easily obtained by substituting the corresponding value of the plate deflection into equation (20). Assuming a pull-in position of $w_{1,pi} \approx 0.415$, as computed using the fifth-order Taylor series expansion method, it can be shown that the corresponding pull-in voltage is given in non-dimensional form by

$$\hat{V}_{b,\mathrm{spi}} = \frac{1.325\,36\sqrt{16.777 + 1.314\,41\hat{\tau}}}{\sqrt{\alpha}}. \tag{26}$$

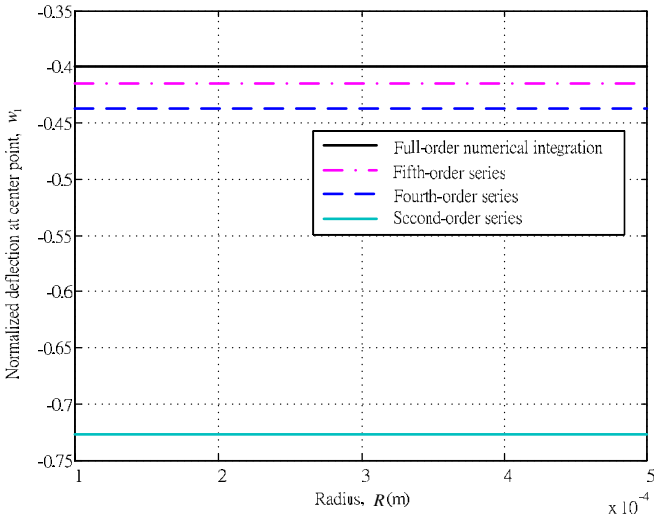

Figure 4. Full-order and finite-order solutions for the static pull-in position in circular plates with various radii.

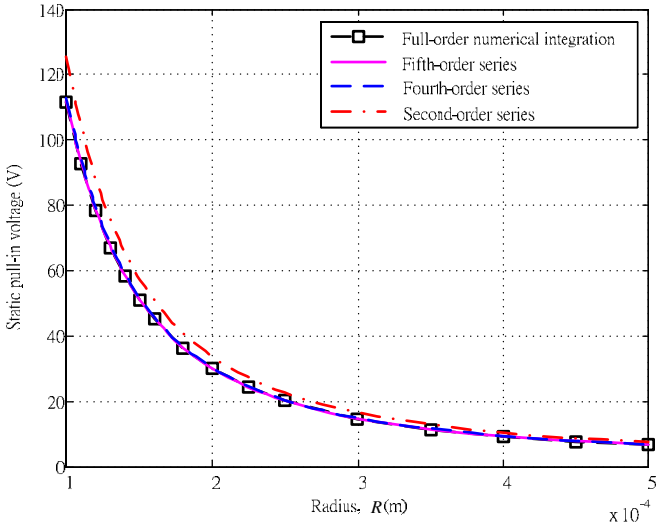

Figure 5. Full-order and finite-order solutions for variation of the static pull-in voltage with respect to the radius of the deformed circular plate.

Converting equation (26) to a dimensional form yields the following expression

$$V_{b,\mathrm{spi}} = \frac{1.325\,36 d^{\frac{3}{2}}\sqrt{16.777 D + 1.314\,41 h R^2 \tau}}{R^2\sqrt{\varepsilon}}. \qquad (27)$$

From an inspection of equation (27), it can be seen that the static pull-in voltage is directly proportional to the square roots of the flexural rigidity, D, the residual stress, τ, and the thickness of the deformed circular micro-plate, h, respectively, but is inversely proportional to the plate radius, R, and the square root of the permittivity of the air gap, ε. Equation (27) indicates that the value of the static pull-in voltage is also significantly influenced by the height of the air gap. Note that contrary to the found dependence of the pull-in voltage on system parameters based on equation (27), the normalized pull-in position is independent of all system parameters, evidenced in equation (25).

Assuming that the parallel plate structure shown in figure 1 has the parameter values indicated in table 1, the closed-form solution of the static pull-in voltage (i.e. equation (27)) yields a value of 20.1792 V. To verify this result, the pull-in voltage is also computed using the full-order Gaussian integration operation to evaluate the electrostatic force acting between the two plates. In this case, the static pull-in voltage is found to be 20.0713 V. Figure 5 compares the results obtained using the full-order integration method and the finite-series Taylor series expansion method for the variation of the static pull-in voltage as a function of the radius of the circular plate. (Note that other than the plate radius, the remaining system parameters are as defined in table 1). In general, it is observed that the value of the pull-in voltage decays exponentially as the radius increases. It can also be seen that the approximation results converge toward the exact solution as the order of the Taylor series expansion increases. In general, the results confirm the feasibility of using the fifth-order approximation of the electrostatic force to compute the static pull-in phenomena and demonstrate the validity of the closed-form solution for the static pull-in voltage given in equation (27).

Table 1. System parameters employed in static and dynamic pull-in analyses.

Symbol	Parameters	Value/unit
h	Deformed circular plate thickness	3.01 μm
L	Circular plate radius	250.0 μm
d	Gap thickness	1.014 μm
ν	Poisson's ratio	0.0436
E	Young's modulus	150.6 GPa

The validity of equation (27) can also be confirmed experimentally. Both Vogl and Nayfeh [12] and Osterberg [19] measured the static pull-in voltages of edge-clamped Silicon micro-circular plates with a thickness of around 3 μm. The height of the air gap was approximately 1 μm in every case. The corresponding results are presented in figure 6 and compared with those computed using the closed-form solution via equation (27) with parameter values of $d = 1.014$ μm, $h = 3.01$ μm, $E = 150.6$ GPa, $\nu = 0.0436$ and $\tau = 7.82$ MPa. From inspection, the average discrepancy between the approximated results and the experimental counterparts is found to be around 2.18%. In other words, the validity of the closed-form solution based on a fifth-order Taylor series expansion is again confirmed.

3.2. Dynamic pull-in prediction

The discussions above have considered the case in which the voltage is gradually increased until the deflection of the center point of the plate reaches a critical displacement and causes the pull-in event to take place. However, in practical applications, the bias voltage is generally applied when the circular plate is in an undeformed condition. As a result, the plate undergoes a rapid deflection, and thus the inertial effects of the plate

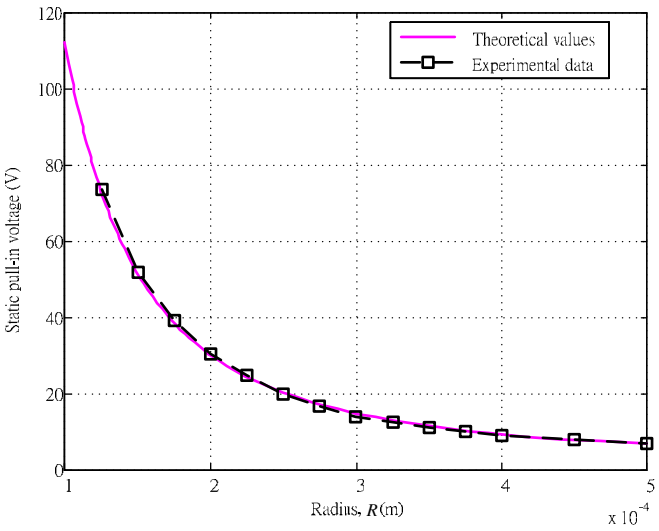

Figure 6. Theoretical and experimental results [12] for variation of static pull-in voltage with respect to the radius of the deformed circular plate.

and the viscosity effect induced by the squeezed air film between the deformed plate and the back plate play roles in determining the occurrence of the pull in event. In the literature, the corresponding bias voltage is conventionally defined as the dynamic pull-in voltage [13, 14].

3.2.1. Energy balance method. Practical capacitive-type MEMS devices are generally actuated using a step voltage signal. The application of this voltage signal causes the deformable plate to overshoot the static equilibrium position considered in the previous analyses. If the overshoot is sufficiently large, the pull-in effect may occur at a voltage lower than that observed in the static case. In analyzing the dynamic pull-in voltage, the actuating voltage signal is modeled as

$$V_b(t) = V_b U(t), \tag{28}$$

where $U(t)$ is a unit step function and V_b is the magnitude of the voltage. Since the parallel plate model shown in figure 1 has a nonlinear nature, examining its response to the step voltage using an analytical technique is usually difficult. Thus, in the present analysis, the dynamic pull-in characteristics of the system are evaluated initially using a simple energy balance method [13, 20].

At time $t = 0$, the system is at rest and has no stored energy. However, when a step voltage is applied, the energy injected into the system is stored as both kinetic and potential energy. Over time, the stored energy above that associated with the equilibrium position is dissipated through damping effects. The energy balance of the system at any instant in time can thus be written as follows:

$$E_{\text{injected}} = E_{\text{kinetic}} + E_{\text{potential}} + E_{\text{dissipated}}. \tag{29}$$

Where E_{injected} is the energy input into the system, E_{kinetic} is the kinetic energy stored in the system, $E_{\text{potential}}$ is the elastic potential energy stored in the system and $E_{\text{dissipated}}$ is the energy lost from the system due to damping effects [13]. In general, the lowest possible value of the dynamic pull-in voltage occurs when the over-shoot reaches its maximum value. In a practical system, the overshoot can be maximized by suppressing the damping effects.

For example, under vacuum conditions, the damping effect within the system is restricted to the material properties of the deformed plate itself, and thus the energy dissipation term in equation (29) can effectively be ignored. When the deformable plate is at the point of maximum overshoot, all of the stored energy is in the form of potential energy since the plate is momentarily at rest, and thus it has zero kinetic energy. The dynamic pull-in event can therefore be evaluated by equating the electrical energy injected into the system with the potential energy associated with the point of maximum overshoot. Therefore, the energy method will be used to analyze the dynamic pull-in phenomenon associated with a step input to the parallel circular plate system.

The dynamic pull-in voltage of the edge-clamped circular plate can be analyzed using the coupled ODEs given in equations (15)–(19) and the energy balance equation given in equation (29). The maximum non-dimensional potential energy stored within the deformed plate can be expressed as

$$\hat{E}_{\text{potential}} = \tfrac{1}{2}\,\mathbf{K}\mathbf{w}_{\max}^2 \approx \tfrac{1}{2} k_1 w_{1,\max}^2, \tag{30}$$

where k_1 is given in equation (18) and $w_{1,\max}$ is the deflection of the plate at the maximum overshoot position. Meanwhile, the non-dimensional energy injected into the system by the applied voltage can be found by integrating the electrostatic force acting on the deformed plate over the plate displacement, i.e.

$$\hat{E}_{\text{injected}} = \int_0^{\mathbf{w}_{\max}} \mathbf{f}_{\mathbf{e}} d\mathbf{w} \approx \int_0^{w_{1,\max}} f_{e,1}\, \mathrm{d}w_1, \tag{31}$$

where $f_{e,1}$ is given in equation (19). Combining equations (29)–(31) and setting the kinetic and dissipated terms equal to zero, the step voltage can be expressed as the following function of the maximum overshoot displacement:

$$\begin{aligned}\hat{V}_b = \big[\big\{-(52.18 + 4.0881\hat{\tau})w_{1,\max}^2\big\}\big/\big\{\alpha\big(0.663\,10 w_{1,\max} \\ - 0.5 w_{1,\max}^2 + 0.4176 w_{1,\max}^3 - 0.3658 w_{1,\max}^4 \\ + 0.3295 w_{1,\max}^5 - 0.3021 w_{1,\max}^6\big)\big\}\big]^{\frac{1}{2}}.\end{aligned} \tag{32}$$

Taking the derivative of equation (32) and setting it equal to zero $\left(\text{i.e. } \frac{\mathrm{d}\hat{V}_b}{\mathrm{d}w_{1,\max}} = 0\right)$ gives

$$w_{1,\max} = -0.641\,346. \tag{33}$$

Note that the negative sign in equation (33) simply indicates a defection of the deformed circular plate in the downward direction. In other words, the magnitude of the position of the local maximum deflection is $w_{1,pi,\max} = 0.641\,346$, i.e. it lies in the range $0 < w_{1,pi,\max} < 1$. In other words, the normalized dynamic pull-in position has a value of around 0.641. It is noted that this value is higher than that observed in the static analyses, i.e. 0.415 (using the finite-order Taylor series expansion method) and 0.408 (using the full-order Gaussian integration method), respectively. As stated above, the minimum value of the potential required to induce the pull-in event is associated with the maximum overshoot position. In other words, the step voltage corresponding to the maximum

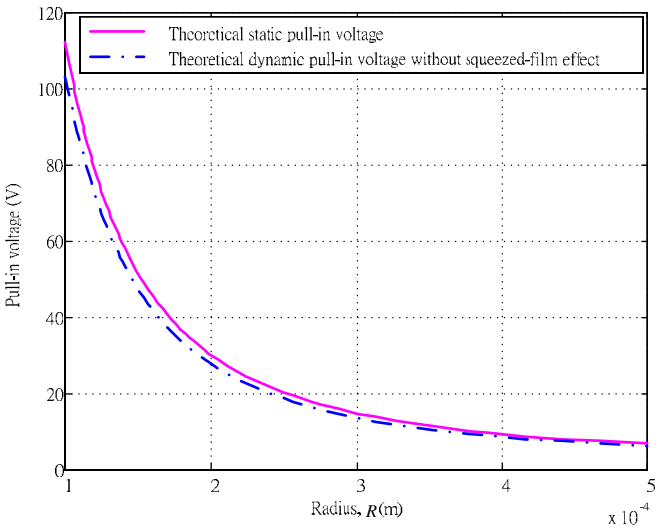

Figure 7. Theoretical static pull-in and theoretical dynamic pull-in voltages without squeezed-film effect considered in the circular plates with various radii.

overshoot defined in equation (33) can be regarded as the dynamic pull-in voltage. Having computed the value of the dynamic pull-in position, the dynamic pull-in voltage is easily obtained by substituting the solution of equation (33) into equation (32), which yields

$$V_{b,\mathrm{dpi}} = \frac{1.219\,789 d^{\frac{3}{2}}\sqrt{16.777D + 1.314\,41hR^2\tau}}{R^2\sqrt{\varepsilon}}. \quad (34)$$

It can be shown that the ratio between the dynamic pull-in voltage, $V_{b,\mathrm{dpi}}$, computed in equation (34) and the static pull-in voltage, $V_{b,\mathrm{spi}}$, computed in equation (27) is given by

$$\frac{V_{b,\mathrm{dpi}}}{V_{b,\mathrm{spi}}} \cong 0.9203. \quad (35)$$

In other words, for the ideal case of zero damping, the dynamic pull-in voltage is approximately 92.03% of the static pull-in voltage. Equation (35) also shows that the value of this ratio is independent of the device parameters. Figure 7 illustrates the variation in the closed-form solutions for the static and dynamic pull-in voltages, respectively, as a function of the plate radius. From a close inspection, it is confirmed that in the ideal zero-damping case the ratio of 92.03% between the static and the dynamic pull-in voltages is maintained irrespective of the plate radius.

At this point, the closed form of the dynamic pull-in voltage prediction of the edge-clamped circular plate is obtained by using the energy method to analyze the dynamic behavior, but it has a shortcoming that it uses the energy method to obtain the dynamic pull-in voltage closed form of the device. The energy method cannot analyze the damping factor of the system. In consequence, the damping-like squeezed-film effect of the system or device cannot be analyzed via the afore-proposed energy method.

3.2.2. Finite-order approximation method. Although the energy balance approach provides a convenient means of evaluating the dynamic pull-in position and voltage, it necessarily makes the assumption that the system has no damping effects. However, in practice, the deflection of the upper plate is resisted by a squeezed-film effect within the air gap as it deforms. Furthermore, the material properties of the upper plate also induce a slight energy dissipation effect. As a result, the value of the pull-in voltage increases slightly since it is necessary to overcome these damping effects in order to induce the pull-in event. In other words, the closed-form solutions obtained in the previous section using the energy balance method can be regarded as representing the ideal case in which neither the material of the plate nor the air gap exerts a damping effect. To model the more realistic case in which damping effects are present within the system, this section of the paper develops a finite-order approximation method to establish the dynamic pull-in response of the parallel plate structure shown in figure 1.

When the squeeze-film effect of the air gap between the two plates is taken into account, the governing equation of motion for the deformed plate can be expressed as

$$\rho h\frac{\partial^2 w}{\partial t^2} + 2c\frac{\partial w}{\partial t} + D\nabla^4 w = \frac{1}{r}\frac{\partial}{\partial r}\left(\frac{\partial w}{\partial r}\frac{\partial \Phi}{\partial r}\right) + \frac{\tau h}{r}\frac{\partial}{\partial r}\left(r\frac{\partial w}{\partial r}\right) + F_e - P, \quad (36)$$

where

$$\nabla^4 w = \left(\frac{\partial^2}{\partial r^2} + \frac{1}{\hat{r}}\frac{\partial}{\partial r}\right)\left(\frac{\partial^2 w}{\partial r^2} + \frac{1}{\hat{r}}\frac{\partial w}{\partial r}\right).$$

In this equation, $w = w(r, t)$ is the deflection of the deformed circular micro-plate; r is the radial coordinate position; h, c and ρ are the thickness, material damping coefficient and density of the circular plate, respectively; τ is the uniform residual biaxial plane stress per unit distance of the deformed micro-plate; D is the flexural rigidity of the plate; E and ν are Young's modulus and Poisson ratio of the circular plate, respectively; F_e is the electrostatic force per unit area of the deformed plate; and P is the net pressure acting on each area of the deformed plate as a result of the squeezed air film effect.

In general, the pressure induced within a thin air film squeezed between two moving plates can be described using the 2D Reynolds equation. This equation is derived from the Navier–Stokes equation under three basic assumptions, namely (1) the inertial terms are negligible compared to the viscous terms, (2) the pressure is constant within the film and (3) the flow in the direction perpendicular to the plates is negligible [21]. Under these conditions, the Reynolds equation can be formulated as follows:

$$\frac{\partial}{\partial x}\left(\frac{\rho_a h_a^3}{12\eta}\frac{\partial P}{\partial x}\right) + \frac{\partial}{\partial y}\left(\frac{\rho_a h_a^3}{12\eta}\frac{\partial P}{\partial y}\right) = \frac{\partial(\rho_a h_a)}{\partial t}, \quad (37)$$

where η and ρ_a are the viscosity and density of the air, respectively; P is the pressure; and h_a is the thickness of the air film. In MEMS applications such as that considered in the present study, the ratio between the mean free path of the air particles and the film thickness (Knudsen number K_n) is sufficiently large that a non-slip boundary condition at the interface between the air and the moving plates is no longer applicable. In practice, the viscosity parameter

η is therefore replaced by an effective viscosity parameter $\eta_{\text{eft}} = \eta(1 + 6K_n)^{-1}$.

The present analysis is based upon a simplified squeezed-film model, in which an assumption is made that the compressibility effects of the air gap are sufficiently small that they can be neglected, i.e. the density of the air, ρ_a, has a constant value. Therefore, the squeezed-film force exerted on the deformed plate by the air within the gap between the two plates can be approximated as an air spring force and a dissipative damping force. For the case of two radially symmetrical parallel circular plates separated by an air gap with constant density and viscosity, the squeezed-film pressure, P, can be expressed as

$$P = \frac{3\eta_{\text{eft}}}{d^3}(R^2 - r^2)\frac{\partial w}{\partial t}, \tag{38}$$

where $w = w(r, t)$ is the deflection of the deformed plate and d is the height of the air gap between the two plates. Substituting equation (38) into the governing equation given in equation (36) yields

$$\rho h\frac{\partial^2 w}{\partial t^2} + \left(2c + \frac{3\eta_{\text{eft}}}{d^3}(R^2 - r^2)\right)\frac{\partial w}{\partial t} + D\nabla^4 w = \frac{1}{r}\frac{\partial}{\partial r}\left(\frac{\partial w}{\partial r}\frac{\partial \Phi}{\partial r}\right) + \frac{\tau h}{r}\frac{\partial}{\partial r}\left(r\frac{\partial w}{\partial r}\right) + F_e. \tag{39}$$

Therefore, it is well known that the squeezed-film force can be reduced to the air spring force by equation (39). For analytical convenience, equation (39) can be transformed into the following non-dimensionalized form:

$$\frac{\partial^2 \hat{w}}{\partial \hat{t}^2} + \left(2\hat{c} + \frac{3R^4\eta_{\text{eft}}}{d^3\sqrt{D\rho h}}(1 - \hat{r}^2)\right)\frac{\partial \hat{w}}{\partial \hat{t}} + \hat{\nabla}^4\hat{w} = \hat{\tau}\frac{1}{\hat{r}}\frac{\partial}{\partial \hat{r}}\left(\hat{r}\frac{\partial \hat{w}}{\partial \hat{r}}\right) + \alpha\hat{F}_e. \tag{40}$$

Applying the Galerkin decomposition method to equation (40) yields the following coupled set of nonlinear modal ODEs for the micro-plate structure with a squeezed-film effect:

$$\mathbf{M}\ddot{\mathbf{w}} + \hat{\mathbf{C}}\dot{\mathbf{w}} + \mathbf{K}\mathbf{w} = \mathbf{f_e}, \tag{41}$$

where the damping term $\hat{\mathbf{C}}$ has the form

$$\hat{c}_k = \left[2\hat{c}\int_0^1 \phi_k^2\,\mathrm{d}\hat{r} + \frac{3R^4\eta_{\text{eft}}}{d^3\sqrt{D\rho h}}\int_0^1 (1 - \hat{r}^2)\phi_k^2\,\mathrm{d}\hat{r}\right], \quad 1 \leqslant k \leqslant N. \tag{42}$$

Considering the first deflection mode only, equation (41) can be rewritten in the following state-space form:

$$\begin{aligned} \dot{x}_1 &= x_2, \\ \dot{x}_2 &= \frac{1}{m_1}[f_{e,1} - \hat{c}_1 x_2 - k_1 x_1], \end{aligned} \tag{43}$$

As in the static analyses performed in section 3.1, the electrostatic force $\hat{F}_e$ associated with the first deflection mode can be computed by applying the fifth-order Taylor series expansion prior to performing the integration operation. Equation (43) can thus be further derived as

$$\begin{aligned} x_2 &= \dot{w}_1, \\ \dot{x}_2 &= \mu_1 + \mu_2 x_1 + \mu_3 x_1^2 + \mu_4 x_1^3 + \mu_5 x_1^4 + \mu_6 x_1^5 + \mu_7 x_2, \end{aligned} \tag{44}$$

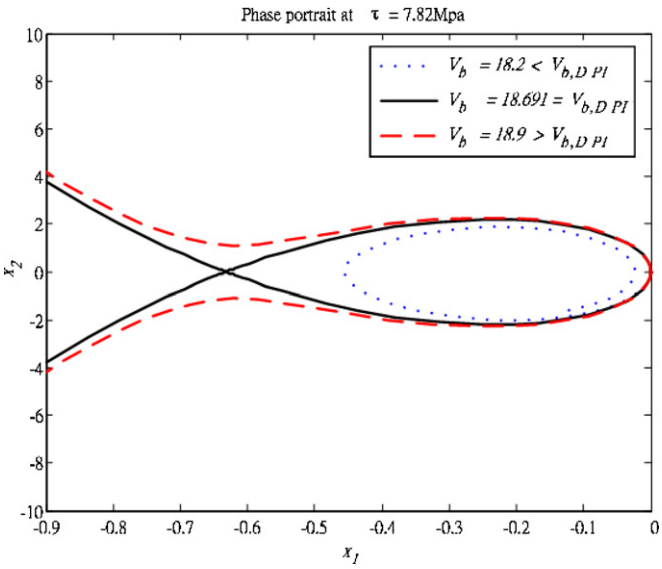

Figure 8. Phase portraits of the system with squeezed-film effects under three bias voltages.

where

$$\begin{aligned} \mu_1 &= -0.663\,103\alpha V_b^2, & \mu_2 &= \alpha V_b^2 - 104.36 - 8.176\,15\hat{\tau}, \\ \mu_3 &= -1.252\,71\alpha V_b^2, & \mu_4 &= 1.463\,18\alpha V_b^2, \\ \mu_5 &= -1.647\,23\alpha V_b^2, & \mu_6 &= 1.812\,81\alpha V_b^2, \\ \mu_7 &= -(2\hat{c} + 0.915\,694B), & B &= \frac{3\eta_{eft}R^4}{d^3\sqrt{D\rho h}}. \end{aligned} \tag{45}$$

Utilizing a numerical method to solve equation (44), the deflection and velocity of the center point of the deformed plate can be calculated for any specified set of system parameters. By plotting x_2 against x_1, a phase portrait can then be obtained from which both the dynamic pull-in voltage and the dynamic pull-in position can be directly derived. Figure 8 presents the phase portraits obtained when solving equation (44) using the parameter values indicated in table 1 and three different values of the bias voltage, V_b. Note that the residual stress is assumed to have a value of 7.82 MPa in every case. Note also that the notation $V_{b,\text{dpi}}$ in the legend denotes the pull-in voltage. It is observed that the three orbits in the figure have quite different characteristics. For example, when a bias voltage of 18.2 V is applied, the orbit forms a closed structure, indicating that the system is in a stable condition. However, at a slightly higher voltage of 18.691 V, a homoclinic orbit is formed, indicating that the voltage corresponds to the dynamic pull-in voltage. The x-axis coordinate of the intersection point indicates the dynamic pull-in position. From inspection, the dynamic pull-in position is found to have a value of 0.6 in the current case. When the voltage is increased beyond the pull-in voltage, the micro-plate collapses, as indicated by the red dashed orbit shown in figure 8.

Figure 8 also confirms the feasibility of using the finite-order approximation method to derive the dynamic pull-in voltage of the capacitive-type system shown in figure 1 for the case where a squeezed-film effect exists between the two plates. Furthermore, the figure shows that the value of the

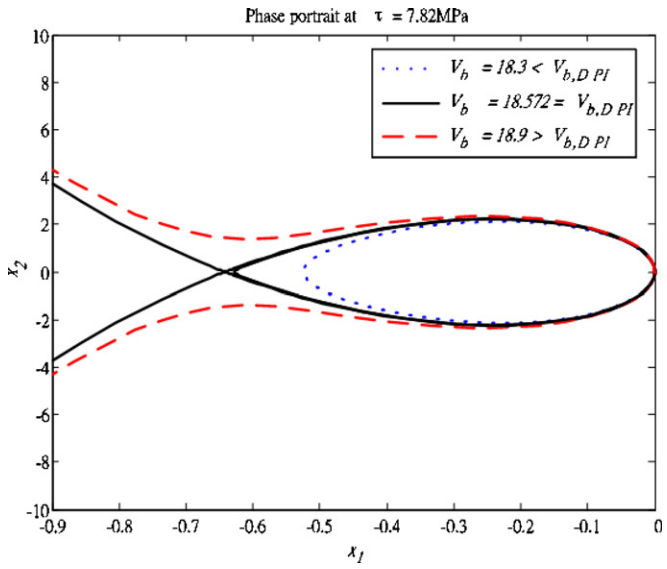

Figure 9. Phase portraits of the undamped system under three bias voltages.

dynamic pull-in voltage is lower than the static pull-in voltages determined in section 3.1, but is higher than that obtained using the energy balance method in which a zero damping effect is assumed. However, this method is unable to obtain a closed-form solution of the dynamic pull-in voltage.

The validity of the finite-order approximation method can be confirmed by setting the damping term to zero and then comparing the results obtained for the dynamic pull-in voltage and position with those obtained using the energy balance method. Considering the structure shown in figure 1, described by the governing equation given in equation (1), figure 9 shows the phase portraits of the undamped system under three values of the applied voltage. (Note that the device parameters and residual stress value are identical to those considered in figure 8). In this case, it can be seen that the dynamic pull-in voltage has a value of $V_{b,\mathrm{dpi}} = 18.572$ V. As expected, the value of the pull-in voltage is lower than that observed in figure 8 ($V_{b,\mathrm{dpi}} = 18.691$ V) since the effects of damping are ignored in figure 8. Comparing the pull-in voltage value of 18.572 V computed using the finite-approximation method under a zero damping assumption with the value of 18.5719 V calculated for the ideal non-damped case, the ratio between them is found to be 99.999 46. In other words, the two methods provide virtually identical results for the dynamic pull-in voltage in a perfectly undamped system. Thus, it can be inferred that in an ideal system, the energy balance method provides a convenient means of determining the dynamic pull-in voltage since it obtains accurate results without the need for complex numerical computations.

3.3. Analysis of pull-in predictions

Having established various theoretical prediction methods for the static and dynamic response of the edge-clamped circular micro-plate configuration shown in figure 1, this section utilizes these methods to examine the respective effects of the system parameters on the pull-in characteristics of the deformable circular plate.

Figure 10(*a*) illustrates the variation of the static and the dc dynamic pull-in voltage (with and without a squeezed-film effect) as the radius of the circular plate, R is increased. (Note that the other parameters are as shown in table 1). Meanwhile, figure 10(*b*) shows the ratios of the dynamic pull-in voltages with and without a squeezed film effect, respectively, to the static pull-in voltage at various values of the plate radius. Finally, figure 10(*c*) shows the variation of the ratio of the dynamic pull-in voltage without a squeezed-film effect to that with a squeezed-film effect as the plate radius is increased. In general, figure 10(*a*) shows that the static and dynamic pull-in voltages all decrease as the radius of the circular plate increases. This result is to be expected since the rigidity of the plate decreases as its radius increases. Moreover, it can be seen that the static pull-in voltage is greater than both dynamic pull-in voltages. Figure 10(*b*) shows that the ratio of the dynamic pull-in voltage without squeezed-film effects to the static pull-in voltage remains constant at a value of around 92.03% irrespective of the value of R. However, it is apparent that the ratio increases when the squeezed-film effect is taken into consideration, particularly at higher values of the plate radius. Although figure 10(*a*) seems to show a very close agreement between the two values of the dynamic pull-in voltages, figure 10(*c*) shows that the ratio of the dynamic pull-in voltage with no squeezed-film effect to that of the pull-in voltage with a squeezed-film effect actually reduces from 100% to 94.3% as the radius of the circular plate is increased from 1 μm to 5 μm.

In practice, the pull-in voltage of the circular plate structure shown in figure 1 is affected not only by the radius of the deformed circular plate, but also by the height of the air gap between the two circular plates and the thickness of the deformed circular plate. Figures 11(*a*)–(*c*) show the effects of the air gap on the static and dynamic pull-in voltages of the device, the ratios of the dynamic pull-in voltages to the static pull-in voltage and the ratio of the dynamic pull-in voltage without a squeezed-film effect to that with a squeezed-film effect, respectively. Figure 11(*a*) shows that the static and dynamic pull-in voltages all increase with an increasing gap height. This result is to be expected since for a constant electrical voltage, the electrostatic force decreases as the gap height increases, and thus a higher electrical voltage is required to induce the pull-in effect. Figure 11(*a*) also confirms that the static pull-in voltage is consistently higher than the two dynamic pull-in voltages. Figure 11(*b*) reveals that in the absence of a squeezed-film effect, the ratio of the dynamic pull-in voltage to the static pull-in voltage has a constant value of 92.03%, irrespective of the gap height. However, it can be seen that when the squeezed-film effect is taken into account, the value of the ratio increases slightly. Figures 11(*b*) and (*c*) both indicate that the relative influence of the squeezed-film effect on the pull-in voltage reduces as the height of the air gap increases.

Figures 12(*a*)–(*c*) illustrate the effect of the thickness of the deformed circular plate on its static and dynamic pull-in characteristics. Figure 12(*a*) shows that the static and dynamic

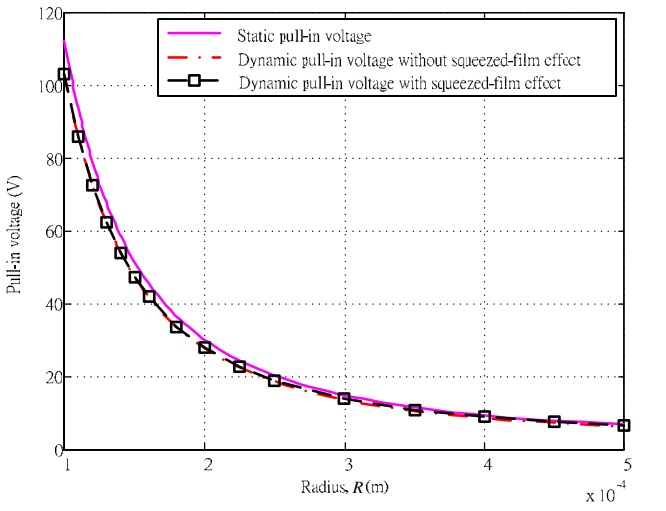

(*a*)

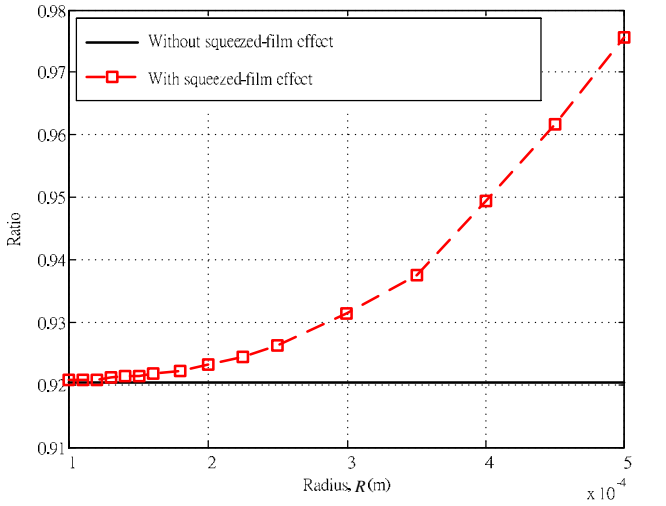

(*b*)

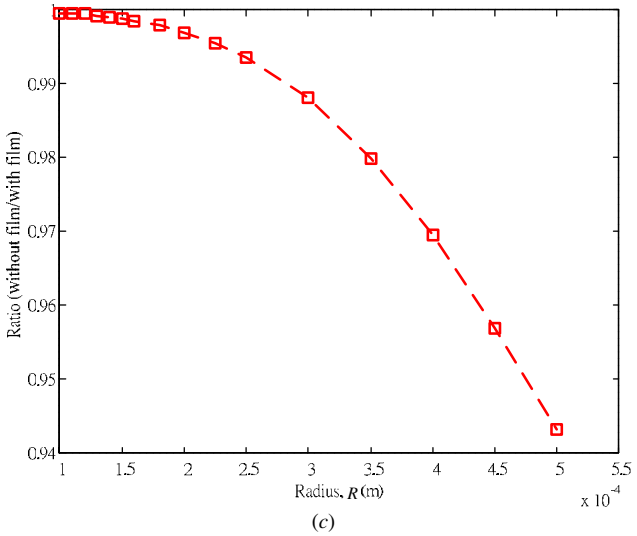

(*c*)

Figure 10. (*a*)–(*c*) Pull-in voltage analyses as a function of the radius of the circular plate.

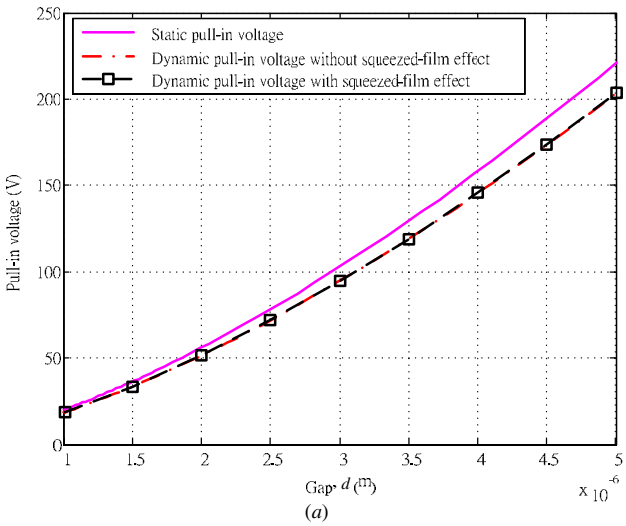

(*a*)

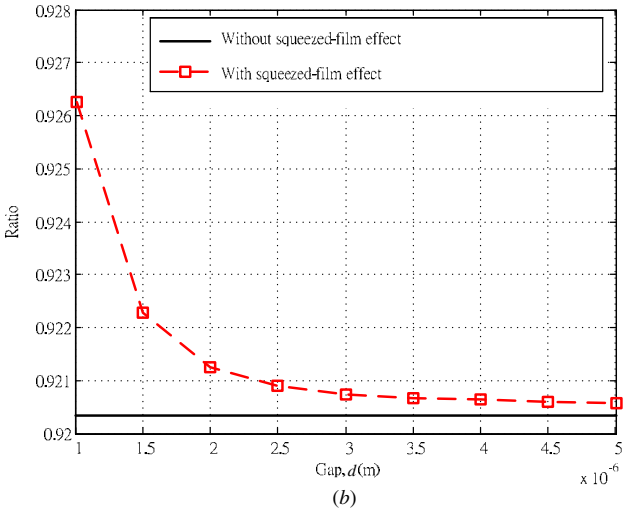

(*b*)

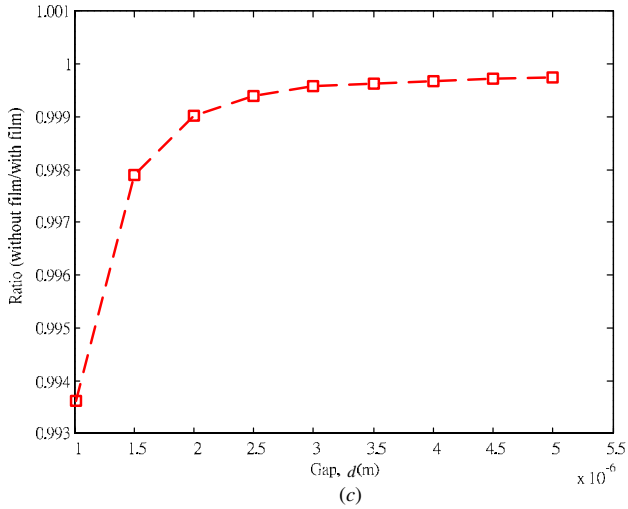

(*c*)

Figure 11. (*a*)–(*c*) Pull-in voltage analyses as a function of the air gap between two circular plates.

pull-in voltages increase as the thickness of the circular plate increases. Intuitively, this is reasonable since the rigidity of the plate is enhanced as its thickness increases. It is seen from figure 12(*a*) that all two dynamic pull-in voltages are close to each other and smaller than the static counterpart. Figure 12(*b*) confirms that the ratio of the ideal dynamic pull-in voltage to

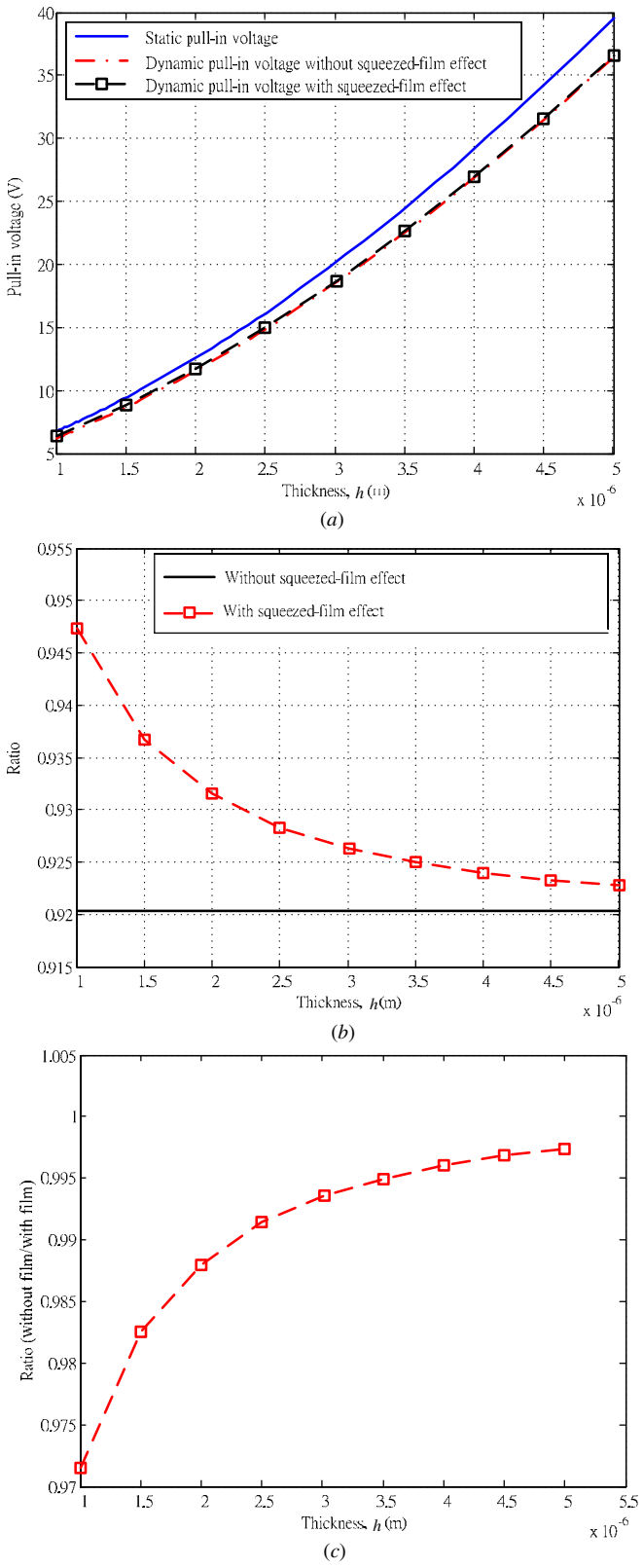

Figure 12. (*a*)–(*c*) Pull-in voltage analyses as a function of the thickness of a deformed circular plate.

the static voltage remains constant at 92.03%. Furthermore, from figures 12(*b*) and (*c*), it can be seen that the influence of the squeezed-film effect on the value of the dynamic pull-in voltage reduces as the thickness of the deformed circular plate increases.

Overall, the results presented in figures 10–12 indicate that the magnitudes of the static pull-in voltage and the dynamic pull-in voltage vary as a function of the radius and thickness of the deformed circular plate and the height of the air gap, respectively. Specifically the pull-in voltage increases with a decreasing plate radius and an increasing plate thickness and air gap. Furthermore, it has been shown that the squeeze damping effect arising as a result of the air film between the two circular plates results in a slight increase (less than 10%) in the dynamic pull-in voltage, particularly at higher values of the plate radius, or lower values of the plate thickness and gap size, respectively.

4. Finite element analysis and validation of theoretical predictions

In order to validate the results presented in section 3 for the static and dynamic pull-in voltages of the two circular micro-plates, this section performs a finite element analysis using the commercial Intellisuite modeling and simulation package. The analysis procedure basically involves solving a coupled system of mechanical and electrical fields. In general, Intellisuite offers two alternative computational schemes, namely a sequential scheme and a direct scheme. In the sequential method, the dynamics of the mechanical and electrical fields are calculated individually and sequentially, whereas in the direct method, the computational process solves the coupled system directly. Although the latter method is more computationally intensive, it has an improved precision, and is therefore adopted in the present analysis to compute the plate deflection corresponding to different values of the applied voltage [22].

Figure 13(*a*) presents the FEM model of the two parallel circular plates. Note that in performing the deformation simulations, the model is constructed using the parameters defined in table 1 and assumes a residual stress of 7.82 MPa. The FEM modeling and analysis herein are accomplished by the commercial software Intellisuite. The finite elements of the circular plate are created by several default automesh densities. In fact, the FEM modeling adopts the function of auto-meshing provided by the commercial software Intellisuite, with the default mesh value with the convergence criterion set to '0.0001 μm'. This default value is confirmed capable of offering reliable results, since as the convergence criterion is increased to '0.001 μm', the pull-in predictions are only varied less than in 2%.

The objective of the simulations is to determine the voltage at which the pull-in event occurs such that the theoretical values of the static and dynamic pull-in voltages derived in the previous section can be verified. When the pull-in event takes place, the upper plate collapses and makes contact with the fixed back plate. In other words, the air gap at the center point of the deformed plate reduces to zero. Thus, the pull-in voltage is easily derived simply by tuning the voltage until a zero air gap is obtained.

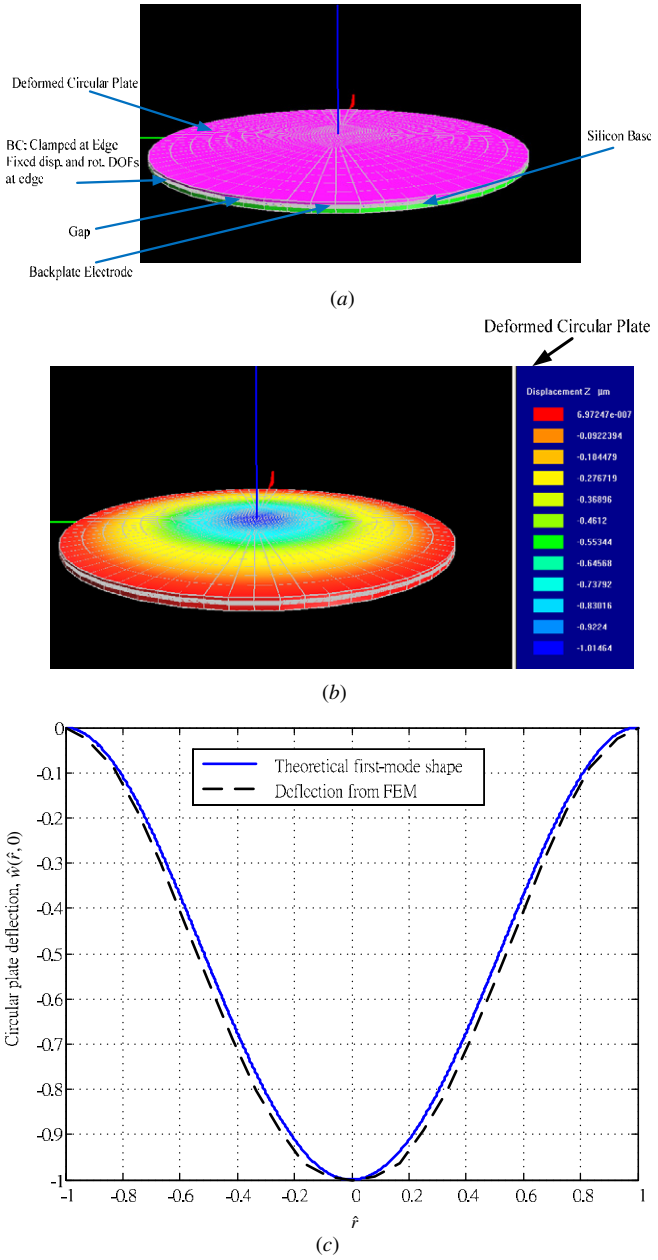

Figure 13. (*a*) Configuration of two parallel circular plates in FEM model; (*b*) deflection of deformed circular plate under applied bias voltage of 19.7 V; (*c*) comparison between FEM and theoretical first-mode approximation results for the circular plate deflection along $\hat{r}$ direction.

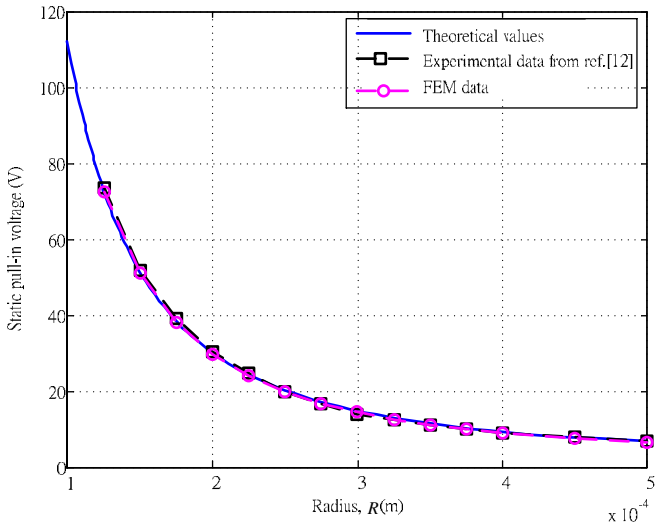

Figure 14. Theoretical, experimental and FEM results for the static pull-in voltages with respect to the radius of the deformed circular plate.

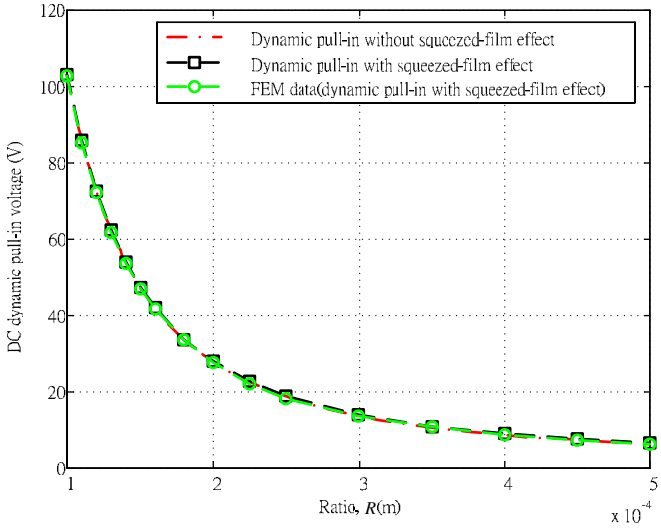

Figure 15. Theoretical results for the dynamic pull-in voltage (with and without squeezed-film consideration) and FEM results for dynamic pull-in voltage (with squeezed-film consideration) at various values of the plate radius.

Figure 13(*b*) presents the deflection of the thin circular plate corresponding to an applied bias voltage of 19.7 V. Under this particular value of the applied bias voltage, the deflection at the center of the plate is seen to be 1.015 μm, i.e. equivalent to the air gap (see table 1). In other words, the FEM analysis predicts a static pull-in voltage of 19.7 V. When the simulation is repeated using an impulse-like application of the applied voltage, the simulation results reveal that the magnitude of the voltage at which the deflection of the center point of the circular plate equals the gap height reduces to 18.2 V, which corresponds to the dynamic pull-in voltage. Utilizing the aforementioned computation and data analysis procedures, the dynamic and static pull-in voltages can be found by FEM.

Figure 13(*c*) illustrates the variation of the normalized circular plate deflection along the $\hat{r}$-axis direction, as computed by the FEM approach and the first-mode approximation method presented in section 3, respectively. Although a slight discrepancy is observed between the two profiles toward the fringes of the plate, the two sets of results are in excellent agreement in the center region. Therefore, the FEM results confirm the effectiveness of the first-mode approximation in predicting the pull-in phenomenon.

Finally, figures 14 and 15 show the theoretical and FEM predictions on static and dynamic pull-in voltages versus plate radius, respectively, along with experimental static pull-in voltages from [12, 19]. It is seen from figure 14 that

theoretical predictions are very close to FEM counterparts. Furthermore, the experimental static pull-in voltages from [12, 19], particularly for the radius at 250 μm, average percentage deviate from the experimental results and the FEM results by just 2.18% and 2.26%, respectively.

The data shown in figure 14 confirm the validity of the theoretical prediction methods established in this study. On the other hand, figure 15 shows the theoretical dynamic pull-in voltages with and without squeezed-film considered, and also the associated FEM data. It is clearly shown in this figure that the results obtained from the reduced-order model for the pull-in voltage subject to a squeezed film effect vary by no more than 2.46% from the results obtained using the FEM approach over the considered radius range. In other words, the validity of the reduced-order model and the finite-approximation method are confirmed.

5. Concluding remarks

This study has developed a reduced-order continuous model to evaluate the pull-in voltage and position of the upper plate in a MEMS structure comprising a parallel arrangement of two circular micro-plates. The magnitudes of the pull-in voltage and the pull-in position have been estimated using various closed-form and numerical techniques. The validity of the theoretical results has been confirmed both experimentally based on available data, and numerically using a FEM approach. The major findings and contributions of the current study can be summarized as follows:

(1) The results obtained using the continuous model with a fifth-order Taylor series expansion of the electrostatic force and a first-mode approximation have indicated that the normalized static pull-in position has a value of 0.415. The equivalent result obtained using the same reduced-order continuous model but a full-order Gaussian integration of the electrostatic force has a slightly lower value of 0.408. In general, the results have shown that the static pull-in position is not only independent of the magnitude of the applied bias voltage, but also of all the system parameters, i.e. the thickness, radius and material of the deformed circular micro-plate and the height of the air gap.

(2) Utilizing the fifth-order Taylor series expansion method and a first-mode approximation, closed-form solutions have been obtained for both the static pull-in voltage and the dynamic pull-in voltage in the ideal case where the parallel circular micro-plate structure has zero damping effects. It has been shown that in this ideal case, the dynamic pull-in voltage is around 92.03% of the static pull-in voltage, irrespective of the plate parameters.

(3) The results obtained using the continuous reduced-order model have shown that the static and dynamic pull-in voltages decrease as the radius of the deformed plate increases, or the plate thickness and air gap height are reduced.

(4) In practice, the air in the gap between the two plates resists the deflection of the upper plate and therefore induces a squeezed-film effect. The results of a finite-order approximation analysis have shown that this squeezed-film effect leads to a slight increase in the value of the dynamic pull-in voltage. The relative influence of the squeezed film increases as the radius of the deformed plate increases, or the plate thickness and air gap height are reduced.

In a future study, the theoretical results obtained for the dynamic pull-in voltage will be validated more rigorously by performing experimental comparisons. Furthermore, the analysis method presented in this study will be extended to the case of MEM capacitor-type devices with square- or beam-type plates.

Acknowledgments

The authors are greatly indebted to the National Science Council of the Republic of China for the supporting research through contact in nos. NSC 97-2221-E-009-057-MY3 and NSC 97-2220-E-009-029, and the National Chip Implementation Center, Taiwan.

References

[1] Pedersen M, Olthuis W and Bergveld P 1997 A silicon condenser microphone with polymide diaphragm and backplate *Sensors Actuators* **63/2** 97–104

[2] Pedersen M, Olthuis W and Bergveld P 1998 High-performance condenser microphone with fully integrated CMOS amplifier and DC-DC voltage converter *J. Microelectromech. Syst.* **7** 387–94

[3] Ho J J, Fang Y K, Hsieh M C, Ting S F, Chen G S, Ju M S, Chen T Y, Huang C R and Chen C Y 2000 Development of a microelectromechanical system pressure sensor for rehabilitation engineering applications *Int. J. Electron.* **87** 757–67

[4] Sallese J M, Grabinski W, Meyer V, Bassin C and Fazan P 2001 Electrical modeling of a pressure sensor MOSFET *Sensors Actuators* **94** 53–8

[5] Chik K D 1997 Precision wavelength light sources for dense WDM system *Proc. SPIE Int Soc. Opt. Eng.* **12** 972–8

[6] Zhu Y and Espinosa H D 2004 Effect of temperature on capacitive RF MEMS switch performance—a coupled-field analysis *J. Micromech. Microeng.* **14** 1270–9

[7] Nadal-Guardia R, Brosa A M and Dehe A 2003 AC transfer function of electrostatic capacitive sensors based on the 1-D equivalent model: application to silicon microphones *J. Microelectromech. Syst.* **12** 972–8

[8] Cheng J, Zhe J and Wu X T 2004 Analytical and finite element model pull-in study of rigid and deformable electrostatic microactuators *J. Micromech. Microeng.* **14** 57–68

[9] Younis M I, Abdel-Rahman E M and Nayfeh A 2003 A reduced-order model for electrically actuated microbeam-based MEMS *J. Microelectromech. Syst.* **12** 672–80

[10] Chao P C P, Chiu C W and Tsai C Y 2006 A novel method to predict the pull-in voltage in a closed form for micro-plates actuated by a distributed electrostatic force *J. Micromech. Microeng.* **16** 986–98

[11] Mehner J E, Gabbay L D and Senturia S D 2000 Computer-aided generation of nonlinear reduced-order dynamic macromodels II: stress-stiffened case *J. Microelectromech. Syst.* **9** 270–8

[12] Vogl G W V and Nayfeh A 2005 A reduced-order model for electrically actuated clamped circular plates *J. Micromech. Microeng.* **15** 684–90

[13] Neilson G N and Barbastathis G 2006 Dynamic pull-in of parallel-plate and torsional electrostatic MEMS actuators *J. Microelectromech. Syst.* **15** 811–21
[14] Elata D and Bamberger H 2006 On the dynamic pull-in of electrostatic actuators with multiple degrees of freedom and multiple voltage sources *J. Microelectromech. Syst.* **15** 131–40
[15] Nayfeh A H and Pai P F 2004 *Linear and Nonlinear Structural Mechanics* (New York: Wiley) pp 501–3
[16] Cheng J, Zhe J and Wu X 2003 Analytical and finite element model pull-in study of rigid and deformable electrostatic microactuators *J. Microelectromech. Syst.* **14** 57–68
[17] Meirovitch L 1967 *Analytical Methods in Vibrations* (London: Macmillan) pp 313–7
[18] O'Neil P V 1995 *Advanced Engineering Mathematics* (California: Brooks/Cole) pp 252–61
[19] Osterberg P M 1995 Electrostatically actuated microelectromechanical test structures for material property measurement *PhD Thesis* Massachusetts Institute of Technology
[20] Neilson G N 2004 Micro-opto-mechanical switching and turning for integration optical system *PhD Dissertation*, Det. Mech. Eng., MIT, Cambridge, MA
[21] Hamrock B J 1994 *Fundamentals of Fluid Film Lubrication* (New Yok: McGraw-Hill)
[22] Chao P C P, Chiu C W and Liu T H 2008 DC dynamic pull-in predictions for a generalized clamped–clamped micro-beam based on a continuous model and bifurcation analysis *J. Micromech. Microeng.* **18** 115008